ADVANCED HEALTHCARE MATERIALS
www.advhealthmat.de

Highly Selective Photothermal Therapy by a Phenoxylated-Dextran-Functionalized Smart Carbon Nanotube Platform

Seungmin Han, Taeyun Kwon, Jo-Eun Um, Seungjoo Haam, and Woo-Jae Kim**

Near-infrared (NIR) photothermal therapy using biocompatible single-walled carbon nanotubes (SWNTs) is advantageous because as-produced SWNTs, without additional size control, both efficiently absorb NIR light and demonstrate high photothermal conversion efficiency. In addition, covalent attachment of receptor molecules to SWNTs can be used to specifically target infected cells. However, this technique interrupts SWNT optical properties and inevitably lowers photothermal conversion efficiency and thus remains major hurdle for SWNT applications. This paper presents a smart-targeting photothermal therapy platform for inflammatory disease using newly developed phenoxylated-dextran-functionalized SWNTs. Phenoxylated dextran is biocompatible and efficiently suspends SWNTs by noncovalent π–π stacking, thereby minimizing SWNT bundle formations and maintaining original SWNT optical properties. Furthermore, it selectively targets inflammatory macrophages by scavenger-receptor binding without any additional receptor molecules; therefore, its preparation is a simple one-step process. Herein, it is experimentally demonstrated that phenoxylated dextran-SWNTs (pD-SWNTs) are also biocompatible, selectively penetrate inflammatory macrophages over normal cells, and exhibit high photothermal conversion efficiency. Consequently, NIR laser-triggered macrophage treatment can be achieved with high accuracy by pD-SWNT without damaging receptor-free cells. These smart targeting materials can be a novel photothermal agent candidate for inflammatory disease.

1. Introduction

Macrophages are major contributors to chronic inflammation and are commonly found in diseases such as arteriosclerosis, asthma, arthritis, and otitis media.[1] In particular, inflammatory macrophages are capable of inherently aggravating the inflammation process.[1,2] Therefore, macrophages have been important targets for the detection and treatment of inflammatory diseases.[3] These inflammatory diseases can be cured using antibiotics or chemotherapy. However, long-term use of these chronic inflammation therapies can cause side effects, including resistance, nausea, abdominal pain, and rashes. To control the use of antibiotics or handle chemotherapy resistant-diseases, two alternative treatment methods might be recommended. One is a surgical method, and the other is photothermal therapy. Although surgery can directly remove disease, it is not an effective technique against diseases such as chronic otitis media or paranasal sinus cancer, which exist in areas of the body that are difficult to access surgically. Additionally, surgical methods are invasive and present risks for bacterial infection. In contrast, photothermal therapy is a noninvasive and straightforward method that can be used to manage the aforementioned diseases.

Photothermal therapy utilizes heat generated by an adopted platform using light absorbed from the near-infrared (NIR) region.[4] A NIR laser irradiates photothermal agents delivered to an affected area; therefore, it allows the selective destruction of targets in the affected area without damaging adjacent normal cells. NIR is also known to be able to penetrate as deep as 10–30 mm into the skin, which is deeper than far-infrared light penetration, because the absorption of NIR by normal organs is relatively low. Therefore, NIR photothermal therapy can be used for a wide range of therapeutic applications.

For efficient photothermal therapy, it is necessary for a substance to have a high NIR absorption efficiency as well as a high photothermal conversion rate.[5] Most substances that are currently studied for photothermal therapy are nanoparticles 20–300 nm in size, which exhibit high treatment efficacies.[6] Gold nanostructures are generally used for photothermal therapy because they are soluble in water, biocompatible, and easily functionalized.[5,7,8] Single-walled carbon nanotubes (SWNTs) have been extensively studied for biosensor and biomedical applications. In addition, SWNTs have also received much attention as novel photothermal therapy candidates because of their unique optical, physical, and electrical properties.[9,10] SWNTs demonstrate photothermal conversion when

S. Han, Prof. S. Haam
Department of Chemical and Biomolecular Engineering
Yonsei University
Seoul 120-749, Republic of Korea
E-mail: haam@yonsei.ac.kr
Dr. T. Kwon
SKKU Advanced Institute of Nano Technology
Sungkyunkwan University (SKKU)
Suwon 16419, Republic of Korea
J.-E. Um, Prof. W.-J. Kim
Department of Chemical and Biological Engineering
Gachon University
Seongnam, Gyeonggi-do 461-701, Republic of Korea
E-mail: wjkim@gachon.ac.kr

DOI: 10.1002/adhm.201600015

irradiated by lasers of wavelengths ranging from 700–1100 nm. SWNTs have also been reported to have the highest in vivo tumor uptake and binding affinity among various other intravenously injected nanomaterials; these results may be due to the high SWNT aspect ratio, which may allow them to extravasate through gaps of leaky blood vessels and penetrate tumors more easily than nanoparticles of other shapes.[11]

Robinson et al. showed that, compared with gold nanorods, SWNTs eliminated cancer cells with higher sensitivity to a NIR laser at both lower dosages and lower laser intensities.[12] At equal concentrations of SWNTs and gold nanorods with 808-nm laser excitation, the SWNT absorbance coefficient was 328% higher, and its photon-to-heat conversion efficiency was three times higher than those of the gold nanorods due to its 1D electronic structure.[12] Gold nanostructures have low thermal stability, and this leads gold nanostructures to be rapidly deactivated during heat generation under NIR irradiation.[13] However, SWNTs have thermal stability, strong optical absorption, and high photothermal energy conversion efficiency in the NIR region.[14]

Although SWNTs have been shown to be promising for photothermal therapy, they cannot be easily applied in clinical studies because of several disadvantageous characteristics. (1) SWNT water insolubility leads to agglomeration and bundling, which cause cytotoxicity,[15] low target cell permeability,[10] and irregular absorption wavelength changes[16] that result in low photothermal conversion efficiency. (2) Pristine-SWNT nonspecific targeting leads to unintended normal cell damage in addition to intended target cell damage.[17] The latter is related to the enhanced permeability and retention effect (EPR effect), which allows nanoparticles, including SWNTs, to escape from leaky vasculature and accumulate to a greater extent in cancerous or inflamed regions.[18] However, EPR effect-based nanoparticle targeting is a passive targeting mechanism, as opposed to an active one. Passive targeting methods can have undesirable results, such as damage to normal cells adjacent to cancer or inflammatory cells.[17] As with other nanostructures, it is difficult to actively target SWNTs against regions of cancer or inflammation without using specific receptor molecules. To selectively target cells, SWNT surface modification with receptor molecules (i.e., DNA, antibodies, or polymers) has been studied.[19] However, DNA or antibody surface modifications tend to be cost-ineffective and induce SWNT surface defects that result in destruction of the unique SWNT optical properties and thus in a decrease of SWNT photoconversion efficiency.

To overcome these underlying issues, we devised novel phenoxylated dextran-SWNTs (pD-SWNTs), which are self-enabled without specific receptors to actively target macrophages, and applied them in a photothermal therapy of inflammatory macrophages. We have previously shown that phenoxylated dextran, synthesized by attachment of phenoxy groups onto dextran and used as a biocompatible SWNT suspension agent, could be used to create individually exfoliated dense aqueous SWNT dispersions while maintaining genuine SWNT optical properties.[20] Phenoxylated dextran has aromatic groups leading to a noncovalent π–π stacking with the carbon nanotube surface. The phenoxylated dextran aromatic groups are stacked along the π-electron orbitals of the SWNT surface, which results in the winding of dextran around the SWNTs. This winding of the hydrophilic dextran enables both SWNT water solubility and high colloidal stability by sterically preventing SWNTs from contacting each other. Moreover, pD-SWNT do not exhibit the bundling behavior that can cause limited medical application, as mentioned above.[10] In addition, the specific binding of dextran to scavenger receptors leads to the selective uptake of pD-SWNT by macrophages, which results in targeted treatment without any assistance from other receptor molecules.[8,21] This dextran-scavenger receptor binding phenomena occurs by pattern recognition of the scavenger receptor. In particular, scavenger receptors recognize carbohydrates, lipids, and proteins that are unique to microorganisms and are not produced by the host.[22,23]

Based on these advantages of pD-SWNT, we have shown that the synthesized pD-SWNT only treat macrophages, which are a major cause of the progressive plaque lesions of arteriosclerosis and chronic inflammatory disease, by photothermal ablation without damaging other cells. Herein, we report that pD-SWNT are promising for photothermal therapy specifically targeting arteriosclerosis and chronic inflammatory disease.

2. Results and Discussion

2.1. Characterization of pD-SWNT

In this work, we synthesized pD-SWNT for targeted delivery and photothermal ablation of inflammatory macrophages under NIR laser irradiation. **Figure 1** provides a schematic illustration of the mechanism of our phenoxylated-dextran-functionalized SWNT platform for highly selective photothermal therapy. To use SWNTs for promising photothermal therapy, pristine-SWNTs are wrapped by phenoxylated dextran through π–π interactions of the phenoxy groups in the phenoxylated dextran. pD-SWNTs are able to target macrophage cells by a dextran-scavenger receptor binding process. However, pD-SWNT do not react with scavenger receptor-free cells, such as fibroblasts; during photothermal ablation, NIR irradiation should pass through these cells. Therefore, pD-SWNTs act as biocompatible photothermal therapeutic agents that selectively target macrophage cells.

We first characterized pD-SWNT using atomic force microscopy (AFM), UV–vis–NIR spectroscopy, and photoluminescence (PL) (**Figure 2**), and compared its properties with those of sodium dodecyl sulfate conjugated SWNTs (SDS-SWNT) to investigate the changes in the SWNT properties upon phenoxylated dextran-functionalization. Figure 2a,b shows AFM images of the SDS-SWNT and pD-SWNT, respectively. Both SWNT solutions were dropped on substrates and washed with copious amount of water to remove SWNT suspension agents, i.e., SDS and phenoxylated dextran. As shown in Figure 2a, the diameter of SDS-SWNT, measured by the height of the AFM image, is ≈1.2 nm, and is well matched to the diameter of HiPco SWNT reported in the literature.[24] This result indicates that SDS is removed from SWNT surface and the AFM image represents pristine SWNT. The diameter of pD-SWNT, shown in Figure 2b, is ≈3.4 nm and this value is much larger than that of pristine

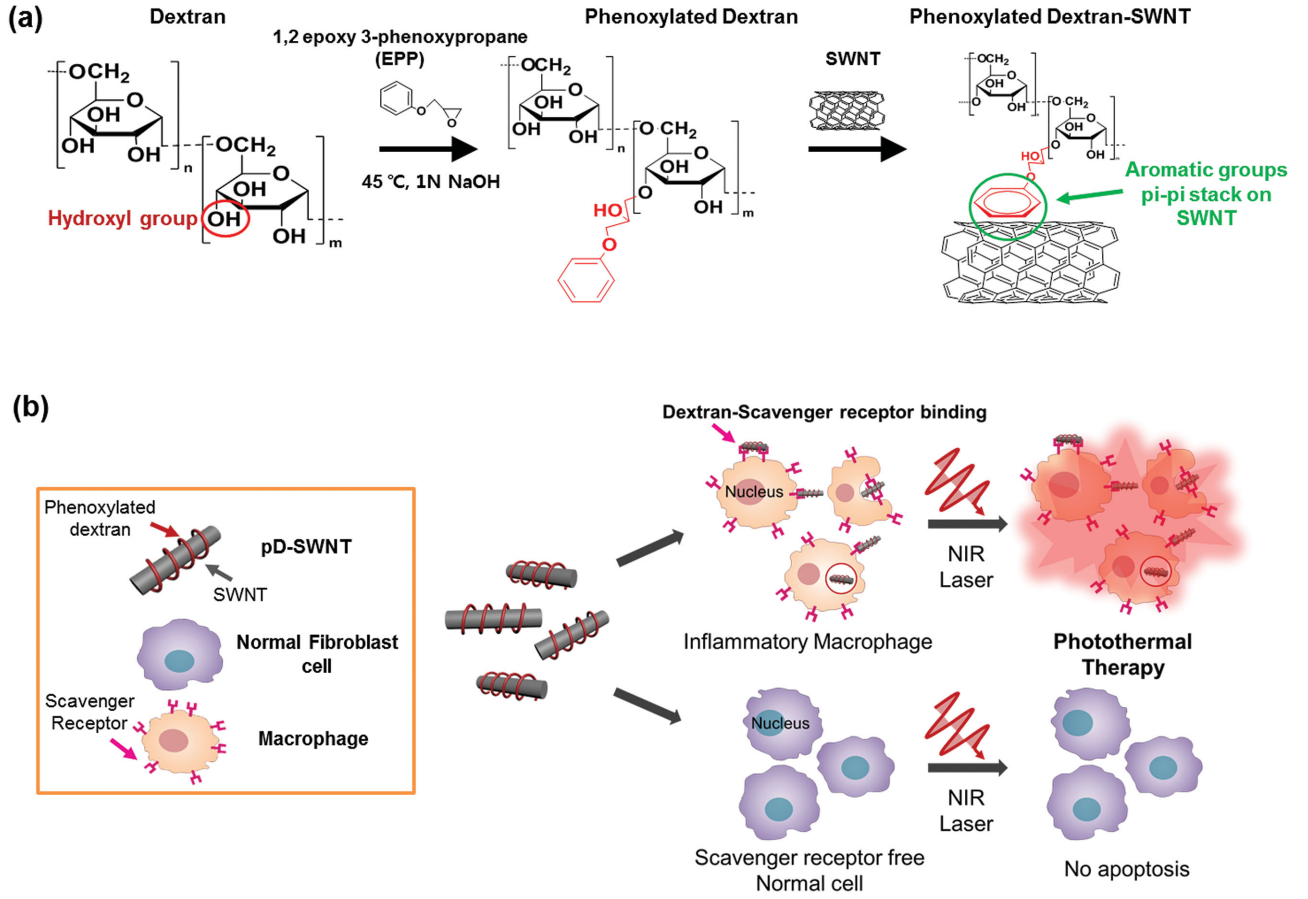

Figure 1. Schematic illustration of a) synthesis of pD-SWNT and b) photothermal therapy specifically targeted against macrophages using pD-SWNT. Phenoxy groups, attached to the dextran molecules by adding EPP, strongly bind to the hydrophobic SWNTs. Phenoxylated dextran is wrapped around SWNT surfaces by π–π stacking, which is noncovalent bonding. The phenoxylated dextran contributes to not only the formation of individually exfoliated SWNTs but also scavenger receptor targeting. Therefore, pD-SWNT only bind macrophages, and they enable photothermal ablation.

SWNT, indicating that the phenoxylated dextran is not removed from SWNT surface and evenly wrapped around SWNT with ≈1.1 nm in height. This value is in good agreement with the height of phenoxylated dextran loop on SWNT, reported in the simulation study by Jeng et. al.[25] These results indicate that phenoxylated dextran strongly binds to the SWNT surface due to the phenoxylated dextran aromatic groups and not easily detach from SWNT surfaces, enabling high colloidal stability of pD-SWNT even in the blood stream of human body, which will be discussed in the later part of this study. Figure 2d represents UV–vis–NIR absorption spectra of pD-SWNT dispersed in water together with those of SDS-SWNT (Figure 2c) as a reference. Initial SWNT dispersions were purified to remove unexfoliated SWNTs and other impurities using a centrifugation process with two different speeds. Interestingly, the quantity and quality of individually dispersed pD-SWNT were similar for pD-SWNT purified by both high-speed (110,527 *g*) and low-speed centrifugation (16,250 *g*), as indicated by the similar peak intensities and peak broadening. As a comparison, for SDS-SWNT (Figure 2c), which have been commonly used as a SWNT dispersion agent in various applications, the quality and quantity of individually suspended SWNTs purified by high-speed centrifugation are much better than those of SWNTs purified by low-speed centrifugation. For SDS-SWNT, this is because initial raw material SWNT bundles were not effectively removed or exfoliated by low-speed centrifugation. The fact that the quality of individually suspended pD-SWNT is high irrespective of centrifugation speed indicates that phenoxylated dextran effectively isolates and wraps SWNTs in large quantities, leaving only trace amounts of bundled SWNTs. To utilize SWNTs as photothermal therapy agents, the degree of SWNT individualization is critical because the NIR-absorption efficiency of SWNTs is strongly affected by the degree of bundling; SWNT absorption wavelength red-shifts due to bundling, resulting in a mismatch between the SWNT optimum absorption wavelength and the wavelength of the laser. This mismatch will decrease SWNT photothermal conversion efficiency. In this sense, pD-SWNTs are good candidates for photothermal therapy applications. Figure 2e,f shows the PL spectra of various semiconducting SWNTs in solution-phase for SDS-SWNT and pD-SWNT, respectively. As shown, PL features of both samples are similar, except for a red-shift in the PL peaks for pD-SWNT compared to those of SDS-SWNT. This shift is due to the change in the dielectric constant of the media, rather than the SWNT bundle formation, as demonstrated in our previous study.[20] The above results indicate that the pD-SWNTs are not SWNT bundles, but

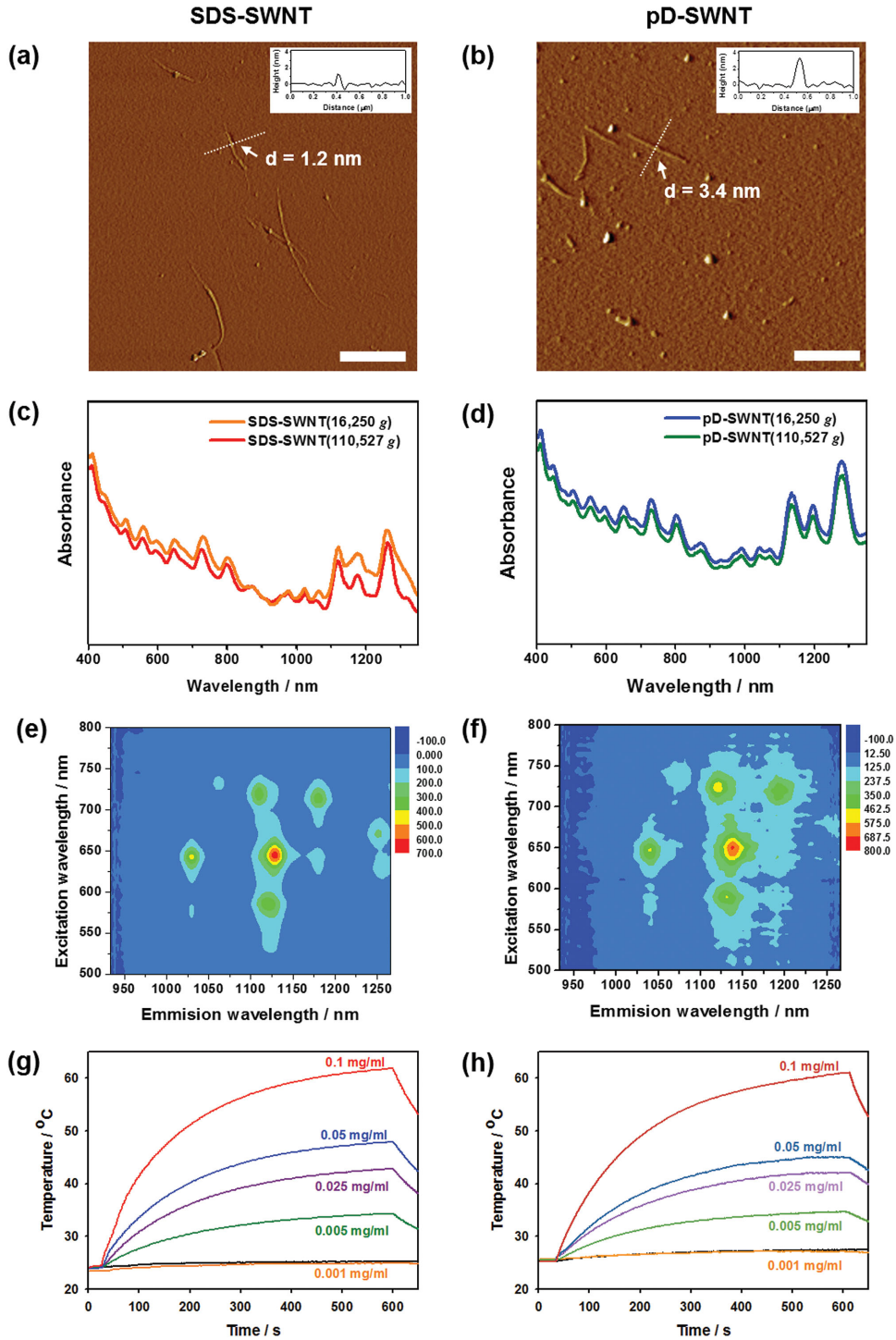

Figure 2. Characterization of SDS-SWNT and pD-SWNT. Left rows (a, c, e, g): SDS-SWNT and right rows (b, d, f, h): pD-SWNT. a,b) AFM tapping mode images, and the scale bar is 1 μm. Inset graphs are the height profiles of pristine SWNT and pD-SWNT measured along the white dotted line of (a) and (b). c,d) UV–vis–NIR absorption spectra of SDS-SWNT and pD-SWNT using ultracentrifuge (110,527 *g*) and microcentrifuge (16,250 *g*). e,f) PL data of SWNTs in solution phase and g,h) Temperature profile for various concentration with an NIR laser (808 nm, 20W cm^{-2}). The laser was turned off after 10 min.

instead they are individualized pD-SWNTs. If the SWNTs were actually bundled, the PL spectra would be quenched by metallic SWNTs, which coexist with semiconducting SWNTs. These results suggest that the pD-SWNTs are individually separated tubes, where individual SWNTs are effectively wrapped in phenoxylated dextran.

To utilize pD-SWNT for photothermal ablation, the photon-to-heat conversion property needs to be verified. Various concentrations of pD-SWNT (0.001, 0.01, 0.025, 0.05, and 0.1 mg mL^{-1}) were placed into individual wells of a 96-well plate and irradiated by a laser (λ = 808 nm, d = 2 mm, 20 W cm^{-2}). When the laser irradiation lasted for 600 s, both the SDS-SWNT and pD-SWNT suspensions showed rapid temperature increases up to 24.9, 34.3, 42.8, 47.9, 61.8 °C (Figure 2g) and 27, 34.7, 42, 45, 61 °C, respectively (Figure 2h). In general, apoptosis by photothermal ablation occurs when the temperature has risen to ≈41–48 °C. In this case, a hyperthermia phenomenon leads to protein unfolding and aggregation that induces the death of only target cells without affecting surrounding cells.[5] Therefore, it was identified that pD-SWNT concentrations exceeding ≈0.025 mg mL^{-1} can generate sufficient heat to induce cell ablation.

Furthermore, stability of pD-SWNT was confirmed to apply pD-SWNT in vitro photothermal therapy (Figure SI3, Supporting Information). pD-SWNT did not show any precipitation after post-24 h incubation in 10% fetal bovine serum (FBS) contained cell culture media condition. UV–vis–NIR absorbance in Figure SI3 (Supporting Information) also suggests that serum condition does not affect pD-SWNT. Altogether, pD-SWNT is appropriate for photothermal therapy without agglomeration in serum condition.

2.2. Intracellular pD-SWNT Interactions

Prior to in vitro photothermal ablation experimentation to utilize pD-SWNT for the treatment of inflammation, intracellular pD-SWNT interactions should be investigated. We assessed pD-SWNT cytotoxicity using an 3-(4,5-dimethylthiazoly-2)-2,5-diphenyltetrazolium bromide (MTT) assay, which showed insignificant cytotoxicity; this result is likely due to the biocompatible phenoxylated dextran wrapped around the pD-SWNT (**Figure 3**a). Similar to the results of the photon-to-heat conversion analysis, these results suggest that pD-SWNT do not affect cell death without laser irradiation.

To perform successful photothermal therapy using pD-SWNT, the agent not only needs to exhibit high photon-to-heat conversion efficiency but also excellent selectivity to specifically target inflammatory macrophages. Scavenger receptors are highly expressed on macrophage (RAW 264.7 cells), especially on the surface of inflammatory macrophages, and usually less expressed on fibroblast (NuFF1 cells).[26] Scavenger receptors are known to bind the basic glucose monomer structure of high molecular weight polysaccharides, such as dextran sulfate, carrageenan, lipopolysaccharide (LPS), lipoteichoic acid, and polyphosphates.[22,23] Therefore, the pD-SWNT of this study are also expected to have specific targeting for scavenger receptors on macrophage.[27] This specific targeting does not affect fibroblasts, which do not have dextran binding sites; during photothermal therapy, NIR irradiation should simply pass through them.[23] We assessed pD-SWNT targeting capability using RAW 264.7 macrophage cells and NuFF1 dextran binding site-free cells with both UV–vis–NIR absorption and cross-sectional cellular transmission electron microscopy (TEM) analysis. Because SWNTs absorb visible and infrared light, cells that have taken up pD-SWNT should have unique UV–vis–NIR absorbance. The UV–vis–NIR absorbance of the untreated cells was deducted from that of the pD-SWNT-treated cells. Figure 3b shows that the absorbance spectrum of the RAW 264.7 cells has a peak at the same point as that of the pD-SWNT; this peak is not present in the NuFF1 cell spectrum. These results suggest that pD-SWNTs were taken up only by the RAW 264.7 cells. Furthermore, pD-SWNT-treated RAW 264.7 cells were examined using cross-sectional cellular TEM (Figure 3c). The pD-SWNT observed within the RAW 264.7 cells exhibited diameters and shapes similar to those of the original pD-SWNT (Figure SI3, Supporting Information). This result clearly corroborates the evidence that pD-SWNTs were taken up only by the RAW 264.7 cells and not by the NuFF1 cells. These UV–vis–NIR absorbance and cellular TEM results indicate that dextran triggers pD-SWNT uptake through interactions with the RAW 264.7 scavenger receptors. Moreover, with no scavenger receptors, the NuFF1 cells did not exhibit any cellular uptake of the pD-SWNT (Figure SI4, Supporting Information).

2.3. Determination of Optimal Conditions for Photothermal Ablation

To determine the optimal photothermal ablation condition, various pD-SWNT concentrations, laser power levels, and exposure times were screened on the RAW 264.7 cells. The RAW 264.7

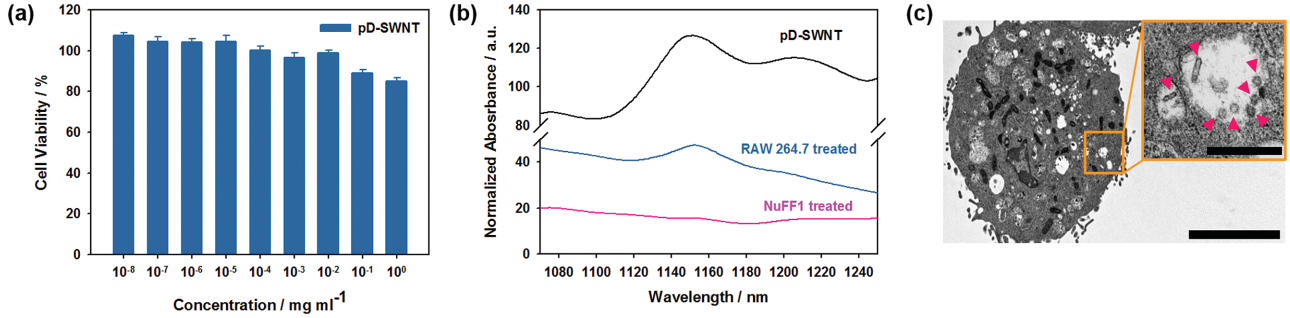

Figure 3. Intracellular interaction and selective targeting of pD-SWNT. a) Cell viability test of RAW 264.7 cells treated with pD-SWNT (n = 6, error bars represent a standard deviation). b) Normalized absorption spectra of RAW 264.7 and NuFF1 cells treated with pD-SWNT. Spectra of cells treated with nanotubes were normalized to the spectra of nontreated cells. c) Cross-sectional TEM images of RAW 264.7 cells incubated with pD-SWNT. The scale bar is 5 μm. The scale bar in the inset image is 500 nm.

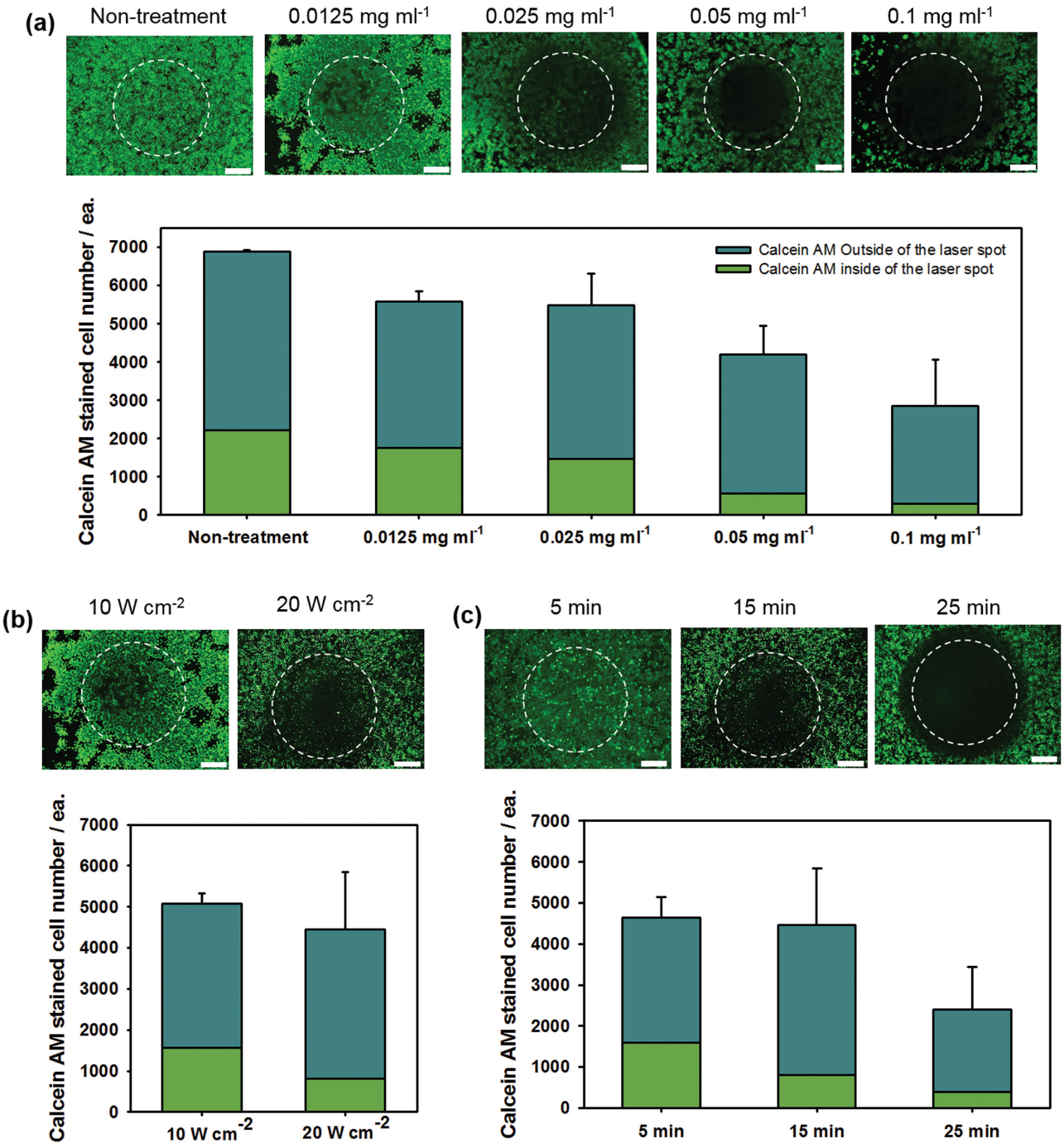

Figure 4. Determination of optimal photothermal ablation conditions. a) Fluorescence images and Calcein AM stained cell counting graph of optimal pD-SWNT concentration for RAW 264.7 cell photothermal therapy. Fluorescence microscopy images of RAW 264.7 cells stained with Calcein AM after treatment with pD-SWNT for 24 h and NIR laser (20 W cm^{-2}, 15 min) irradiation. Calcein AM is labeled with green and stains viable cells. The white dotted curves represent the location of the laser beam. From a graph, dark cyan and gray bars represent alive cells from outside and inside of the laser spot, respectively. 0.1 mg mL^{-1} shows harsh cell death even outside of the laser spot. It indicates that 0.05 mg mL^{-1} is the optimal concentration for photothermal ablation in these conditions. b) Fluorescent images and graph of cells stained with Calcein AM after different NIR laser power exposures. RAW 264.7 cells were incubated with 0.05 mg mL^{-1} of pD-SWNT for 24 h and were subsequently irradiated with different laser powers. A laser power of 20 W cm^{-2} resulted in a higher photothermal ablation effect than a laser power of 10 W cm^{-2}. c) Fluroscence images and Calcein AM stained cell counting graph of photothermal ablation effect depends on laser exposure time. RAW 264.7 cells were irradiated with a laser power of 20 W cm^{-2} for different exposure times after treatment with pD-SWNT (0.05 mg mL^{-1}) for 24 h. When cells were irradiated for 25 min, excessive cell death was observed outside the laser spot. Altogether, the results showed that effective photothermal ablation occurred when 20 W cm^{-2} of NIR laser was irradiated for 15 min after treatment with pD-SWNT (0.05 mg mL^{-1}). All scale bars are 500 μm.

cells were incubated with various concentrations of pD-SWNT (0, 0.0125, 0.025, 0.05, and 0.1 mg mL^{-1}) for 24 h to determine the appropriate treatment concentration (**Figure 4**a). The cells were washed with Dulbecco's phosphate-buffered saline (DPBS) solution and the pD-SWNT solution was replaced with fresh media. Subsequently, the RAW 264.7 cells were stained with Calcein AM after laser irradiation (20 W cm^{-2}, 15 min). Calcein AM emits green fluorescence while it is decomposed by esterase of live cells. We counted Calcein AM stained cells inside (green bar in the Figure 4 graph) and outside (dark cyan bar in the Figure 4 graph) of the laser spot from the fluorescence images using Image J software. As images and graph shown in Figure 4a, the 0.05 mg mL^{-1} of pD-SWNT concentration exhibited the ideal photothermal ablation effect of cell death only occurring inside the laser spot, while 0.1 mg mL^{-1} concentration shows harsh cell death even outside of the laser spot. After determination of the optimal pD-SWNT concentration, laser exposure power and time were investigated (Figure 4b,c). Using estimated laser exposure powers, 20 W cm^{-2} laser power was observed to yield a higher cell ablation effect than lower laser power (e.g., 10 W cm^{-2}). The stronger laser power resulted in pD-SWNT actively emitting thermal energy. Then, RAW 264.7 cells were irradiated for 5, 15, and 25 min with 20 W cm^{-2} of laser power after treatment with pD-SWNT at 0.05 mg mL^{-1} (Figure 4c). Exposure times shorter than 15 min were not sufficient to generate the heat required for ablation. However, harsh cell death was observed even outside the laser spot for exposure times longer than 15 min; these treatments resulted in complete cell death, which is not a localized therapy. From all these results, the most effective photothermal ablation occurred using a NIR laser irradiation power of 20 W cm^{-2} for 15 min after a treatment of 0.05 mg mL^{-1} pD-SWNT for 24 h.

We confirmed the photothermal ablation effects by testing the optimal conditions first without the NIR laser irradiation and then without the pD-SWNT (**Figure 5**). The photothermal ablation of the RAW 264.7 cells was compared with two other conditions: (1) incubation without pD-SWNT followed by NIR irradiation with 20 W cm^{-2} power; and (2) incubation with 0.05 mg mL^{-1} of pD-SWNT without NIR irradiation. Subsequently, the cells were stained with Calcein AM and Ethidium homodimer-1 (EthD-1). EthD-1 stains dead cells by binding to DNA after penetrating damaged cell membranes. We also counted Calcein AM and EthD-1 stained cells to numerically confirm photothermal effect. Green and dark cyan bars represent same parts as Figure 4, additionally red and dark gray bars in Figure 5 represent photothermally affected cell inside and outside of the laser spot, respectively. As shown in Figure 5, because of insignificant cell death inside of the laser spot, the red bar is not shown in the graph when either the pD-SWNT or the NIR laser irradiation was lacking, which means photothermal ablation was not apparent. These results suggest that NIR irradiation does not inherently induce cell death; therefore, it would not affect fibroblasts, which do not have scavenger receptors. In line with the previously discussed MTT assay results, the pD-SWNT have negligible inherent cytotoxicity at a concentration of 0.05 mg mL^{-1}. However, when exposed to NIR laser irradiation, they can emit heat for the targeted treatment of inflammatory macrophages. These results indicate that pD-SWNT show promise to be used as photothermal agents for localized treatment.

2.4. Selective Photothermal Therapy on Inflammatory Macrophages

To further assess the feasibility of using pD-SWNT as therapeutic agents against inflammatory macrophages, we examined the localized thermal ablation of NuFF1, RAW 264.7 cells, and activated RAW 264.7 cells. When RAW 264.7 cells were activated by LPS, it is polarized to inflammatory macrophage which continuously releases inflammatory mediators.[28] Inflammatory macrophage is deeply related with scavenger receptor.[28,29] There are references that nonstimulated macrophage and inflammatory macrophage are composed of inflammation lesion, such as atherosclerosis.[30] On the other hand, NuFF1 cells are fibroblasts which have fewer scavenger receptors

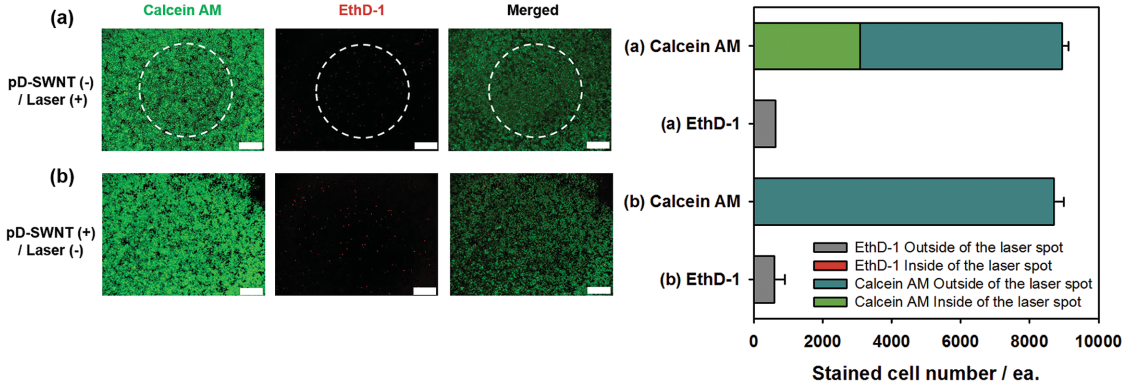

Figure 5. Individual photothermal ablation effects of a) only pD-SWNT or b) NIR irradiation. Fluorescence microscopy images of RAW 264.7 cells stained with Calcein AM and ethidium homodimer-1 (EthD-1). NIR laser was irradiated for 15 min (λ = 808 nm, 20 W cm^{-2}) as the only control for (a). pD-SWNT was treated (0.05 mg mL^{-1}) for 24 h without NIR laser irradiation for (b). The white dotted curves represent the location of the laser beam. Also, the graph shows Calcein AM and EthD-1 stained cells from (a) and (b). Dark gray and dark red represent dead cells from outside and inside of the laser spot, respectively. Dark cyan and gray bars represent alive cells from outside and inside of the laser spot, respectively. Because of insignificant cell death from inside of the laser spot, the dark red bar is not shown in the graph. Individually, NIR irradiation and pD-SWNT do not affect cell damage. The scale bar is 500 μm.

than macrophages.[31] Therefore, it is able to treat inflammation with photothermal therapy by scavenger receptor targeting with pD-SWNT. The cells were incubated with 0.05 mg mL^{-1} of pD-SWNT for 24 h, and they were exposed to an 808-nm laser in vitro (20 W cm^{-2}, 15 min), according to the optimal treatment condition. Subsequently, fluorescence microscopy was used to image Calcein AM and EthD-1 staining (**Figure 6**). The left side of white dotted curve shown is inside the laser spot, and the right side is outside the laser spot. As shown in Figure 6a, a large amount of Calcein AM staining was observed in the NuFF1 cells, while very few cells exhibiting EthD-1 staining were observed, regardless of laser irradiation. In contrast, few RAW 264.7 and activated RAW264.7 cells showed Calcein AM staining, but many cells in the irradiated areas exhibited EthD-1 staining. Additionally, fewer RAW 264.7 and activated RAW 264.7 cells exhibited EthD-1 staining outside the laser spot, which is a demonstration of localized treatment. The data shown in Figure 6b were obtained by counting the number of cells with EthD-1 staining in Figure 6a using Image J. The red and gray bars represent affected cells inside and outside of the laser spot, respectively. In accord with the fluorescent images, Figure 6b also shows the number of RAW 264.7 and activated RAW 264.7 cells with EthD-1 staining to be much larger compared with that of the NuFF1 cells. These results are related with Figure 3b,c, which demonstrated the selective uptake of pD-SWNT by macrophages in situ. This phenomenon occurs by scavenger receptor binding with dextran. Because NuFF1 cells have fewer scavenger receptors, hardly any pD-SWNT uptake occurs, resulting in an imperceptible photothermal ablation effect. To verify that pD-SWNT is delivered to macrophage by scavenger receptor-dextran binding, we confirmed reduction of photothermal cell death and intracellular pD-SWNT uptake when scavenger receptor is blocked by incubation with excess amount of dextran (Figure SI6, Supporting Information). Raw 264.7 cells were incubated with pD-SWNT and Nile Red loaded pD-SWNT in excess amount of dextran contained condition for 24 h at 37 °C. The dextran cotreated cells showed insignificant photothermal ablation, and also low efficiency of pD-SWNT uptake. It implies that pD-SWNT targets scavenger receptor of macrophage. Also, the red bar in Figure 6b is longer than the gray bar, which illustrates the localized pD-SWNT treatment in RAW 264.7 and activated RAW 264.7 cells. Overall, pD-SWNT have been shown to act as photothermal therapy agents that specifically target inflammatory cells, and they could serve to selectively treat only inflammation with localized laser irradiation.

3. Conclusion

In conclusion, we have overcome the problem of nonspecific SWNT targeting, which has been a persistent problem in previous studies, by a simple surface modification with phenoxylated dextran. pD-SWNT can be easily obtained in large quantities using short durations of low-energy centrifuging. Our novel method enables a SWNT application that is both high quality and cost effective. pD-SWNT do not lose their original photon-to-heat conversion ability, even with phenoxylated dextran wrapped around the SWNTs. Moreover, our prepared pD-SWNT showed excellent performance as photothermal therapy agents highly selective for macrophage cells. These pD-SWNT did not harm fibroblasts, even when the fibroblasts were exposed to both pD-SWNT and NIR laser irradiation. Future work should focus on the further development of this method as well as in vivo pD-SWNT photothermal therapeutic effects. Ultimately, this work demonstrates the therapeutic potential of pD-SWNT for many diseases influenced by inflammatory macrophages, including arteriosclerosis and arthritis, among others.

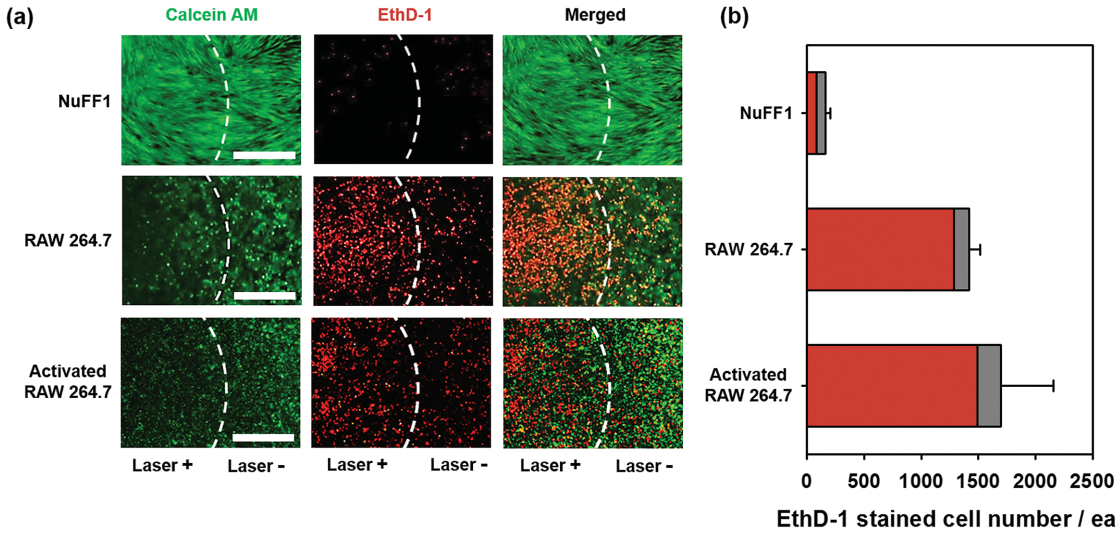

Figure 6. Specifically targeted photothermal therapy effect of pD-SWNT. a) Fluorescence microscopy images of NuFF1, RAW 264.7, and activated RAW 264.7 cells stained with Calcein AM and ethidium homodimer-1 (EthD-1) after treatment with pD-SWNT (0.05 mg mL^{-1}) for 24 h. The NIR laser was subsequently used for durations of 15 min (808 nm, 20 W cm^{-2}) because of the results of the optimal photothermal ablation condition test. Calcein AM and EthD-1 stained viable cells and dead cells, respectively. The white dotted curves represent the location of the laser beam. The scale bar is 500 μm. b) The comparison between NuFF1 and RAW 264.7 cells stained with EthD-1. The graph was based on the results of (a). pD-SWNT clearly demonstrate a photothermal therapy effect on the RAW 264.7 and activated RAW 264.7 cells, but not on the NuFF1 cells.

For future photothermal therapy applications, our phenoxylated-dextran-functionalized smart carbon nanotube platform will be investigated using more realistic samples, including various cells of different diseases.

4. Experimental Section

Materials Synthesis: Commercial SWNTs (NanoIntegris Co. Ltd., USA) were used as a starting material without any purification process and dispersed in aqueous solution with phenoxylated dextran and SDS (Sigma-Aldrich) as a reference. The biocompatible SWNT dispersion agent, phenoxylated dextran, was synthesized using dextran (40 kDa in molecular weight) and 1,2-epoxy-3-phenoxy propane (EPP), which were both purchased from Sigma-Aldrich, following the procedure reported in our previous study.[20] The phenoxy groups on dextran strongly bind to the hydrophobic SWNTs and thus enable stable SWNT suspensions in biological environments; these groups were attached to the dextran molecules by adding EPP in a dextran-dissolved 1 M NaOH solution. The phenoxy content of phenoxylated dextran was adjusted by controlling the injected amounts of EPP. The reaction was performed for 15 h at 45 °C, and the produced phenoxylated dextran was washed with copious amounts of methanol and water to eliminate any unreacted EPP. The phenoxy content of the produced phenoxylated dextran was determined by absorption at 269 nm (ε = 1372 L mol^{-1} cm^{-1}) with a UV–vis–nIR spectrophotometer (Perkin Elmer),[32] and was adjusted to 14 wt%, which was reported to be the optimum composition for the production of high quality SWNT suspensions in our previous study.[20] When equimolar amounts of both reagents were used (8 g of 40 kD dextran and 7.42 g of EPP) under the above experimental conditions, phenoxylated dextran, having ≈14 wt% phenoxy content, was obtained. The SWNTs were dissolved in deionized water (1 mg mL^{-1} concentration) with 1 wt% of phenoxylated dextran or SDS and sonicated for 1 h at a power of 10 W (Sonics); sonication was followed by centrifugation either at 16 250 *g* for 30 min or 110 527 *g* for 4 h to obtain individually suspended phenoxylated dextran-SWNTs and SDS-SWNTs.

SWNT Characterizations: The phenoxy content of the synthesized phenoxylated dextran was determined by its absorption intensity at 269 nm using a UV–vis–NIR spectrophotometer (Perkin Elmer); the prepared pD-SWNT were also characterized using a UV–vis–NIR spectrometer. SWNT morphology was confirmed by scanning probe microscopy (SPM) and TEM analysis. The SPM-based measurements were performed using an Innova (Veeco Inc., Santa Barbara, CA, USA) with a Nanocontroller V (Veeco Inc.) under an ambient condition at room temperature. All SWNT images were acquired using a tapping mode at the scanned location. We utilized a TESP-V2 tip (Veeco Inc.) as a scanning probe. Here, the TESP-V2 tip has a normal resonant frequency of 320 kHz and tip radius of ≈8 nm. The tapping mode atomic-force microscopy (tmAFM) images were acquired using a scanning speed of 1 μm s^{-1}, which is a suitable speed to yield high-quality images. We obtained the tmAFM images using a scan size of 5 × 5 μm, which is a scan size suitable for imaging a few SWNTs on the substrate. All SPM images were generated by Nanoscope software V7.2. The pD-SWNT TEM images were obtained using cross-sectional TEM (JEOL-1100). Cross-sectional cube samples were composed of pD-SWNT-treated cell suspension solution. For stability test of pD-SWNT, 0.05 mg mL^{-1} of pD-SWNT was incubated in 10% FBS contained Dulbecco's Modified Eagle Medium (DMEM) cell culture media for 24 h at 37 °C.

In Vitro Cell Viability Assay: pD-SWNT cytotoxicity against RAW 264.7 cells was evaluated by measuring the inhibition of cell growth using the 3-(4,5-dimethylthiazoly-2)-2,5-diphenyltetrazolium bromide (MTT) assay, which is based on the reduction of 3-(4,5-dimethylthiazoly-2)-2,5-diphenyltetrazolium bromide in metabolically active cells. The RAW 264.7 cells (2 × 10^4 cells per well) were seeded onto 96-well plates and incubated at 37 °C for 24 h. Then, the cells were treated with 100 μL of DMEM (3% FBS) containing pD-SWNT at various concentrations and were subsequently incubated for an additional 24 h. The cells were washed three times with DPBS and were then treated with a yellow MTT solution, where formazan crystals were solubilized with 10% SDS in 0.01 M HCl. The absorbance of purple solution, which results from formazan, was measured at 575 and 650 nm as a reference using a hybrid multimode microplate reader. Consequently, cell viability was determined by the intensity ratio of the treated to nontreated cells and is represented as the average ± standard deviation (n = 6).

Photothermal Conversion Efficacy of pD-SWNT: The photothermal conversion efficiency of the pD-SWNT was confirmed by measuring temperature increases upon laser irradiation. Various concentrations (distilled water, 0.001, 0.01, 0.025, 0.05, and 0.1 mg mL^{-1}) were placed in individual wells of a 96-well plate and treated with an 808-nm NIR laser for 10 min at a density of 20 W cm^{-2}. The temperature of each pD-SWNT solution was monitored by a thermocouple (187 True RMA Multimeter, Fluke).

Cellular Internalization of pD-SWNT: RAW 264.7 cells (4 × 10^5 cells per well) and NuFF1 cells (2 × 10^5 cells per well) were seeded onto 6-well plates for cellular internalization assessment by both UV absorbance and cellular transmission electron microscopy (Cell TEM). After 24 h of incubation, the cells were treated with cell media containing 0.05 mg mL^{-1} of pD-SWNT and were incubated for another 24 h. Subsequently, the cells were washed three times with DPBS, which was followed by cell harvesting using TrypLE solution (Gibco). For the UV absorbance assay, the treated and nontreated cells were fixed with 4% paraformaldehyde solution. The UV absorbance value of the nontreated cells was subtracted from that of the treated cells. pD-SWNT cellular internalization was determined by absorbance value comparisons between the treated and nontreated cells. To prepare cell TEM sample, the harvested cells were fixed with fixation buffer (2% Glutaraldehyde and 2% Paraformaldehyde in 0.1 M phosphate buffer (pH 7.4) solution) for 12 h, and fixation buffer was washed by 0.1 M phosphate buffer. In subsequent, the fixed cells were postfixed with 1% osmium tetroxide (OsO4) contained 0.1 M phosphate buffer for 2 h and dehydrated in ascending gradual series (50%–100%) of ethanol. The dehydrated sample was infiltrated with propylene oxide. The specimens were embedded in Poly/Bed 812 kit (Polysciences) and incubated in electron microscope oven (TD-700, DOSAKA, Japan) at 65 °C for 24 h. After that, section of 200–250 nm thick was cut from resin block and stained with toluidine blue (Sigma, T3260) for light microscope. Observed section was decided from light microscope and resection of ultrathin 70 nm thick was double stained with 6% uranyl acetate (EMS, 22400 for 20 min) and lead citrate (Fisher for 10 min) for contrast staining. The stained ultrathin section was transferred on copper and nickel TEM grids, and observed by TEM (JEOL-1100).

Determination of Optimal pD-SWNT Photothermal Ablation Conditions: The optimal pD-SWNT concentration was first determined. RAW 264.7 cells (1 × 10^5 cells per well) were seeded onto a 48-well plate and incubated for 24 h; they were then exposed to and incubated with various pD-SWNT concentrations (0, 0.0125, 0.025, 0.05, and 0.1 mg mL^{-1}) for an additional 24 h. The cells were irradiated with an NIR laser (808 nm, 20 W cm^{-2}) for 15 min and subsequently washed three times. Then, Calcein AM was used for staining live cells to confirm the appropriate pD-SWNT concentration for photothermal ablation. After determination of the optimal pD-SWNT treatment concentration, NIR laser power and exposure time were optimized for efficient photothermal ablation. The cells were prepared in the manner described above and were then irradiated with different NIR laser powers and exposure times. These factors were assessed by comparison of Calcein AM stained area over laser irradiated area.

In Vitro Photothermal Therapeutic Efficacy of pD-SWNT: RAW 264.7 cells (1 × 10^5 cells per well) and NuFF1 cells (0.5 × 10^5 cells per well) were seeded onto a 48-well plate and incubated for 24 h; they were then incubated with 200 μL of pD-SWNT (0.05 mg mL^{-1}) in cell media at 37 °C for a day. For activated RAW 264.7 cells, RAW 264.7 cells (2 × 10^5 cells per well) were incubated for 24 h in a 48-well plate. After that, the cells were activated by incubation with LPS chemical (1 μg μL^{-1}) for 24 h. Subsequently, activated RAW 264.7 cells (inflammatory macrophage) were treated with 0.5 mg mL^{-1} of pD-SWNT for 24 h. After treatment of pD-SWNT, the cells were rinsed three times with DPBS, and 500 μL

of DMEM was added into each well. For the NIR laser irradiation assay, the cells were exposed to an 808-nm optical diode NIR laser for 15 min at 20 W cm^{-2}. The irradiated cells were washed and stained with Calcein AM and Ethidium homodimer-1 for 30 min to assess cell viability and cytotoxicity. Viable cells were stained by Calcein AM, which has excitation and emission at 494 and 517 nm. However, EthD-1 stains dead cells, and it has excitation and emission at 528 and 617 nm, respectively. The fluorescent images were collected using an optical microscope system (Olympus BX51).

Supporting Information

Supporting Information is available from the Wiley Online Library or from the author.

Acknowledgements

S.H. and Dr. T.K. contributed equally to this work. This work was supported by the Basic Science Research Program of the National Research Foundation of Korea (NRF) and funded by the Ministry of Education (NRF-2013R1A1A2061805), and also supported by BioNano Health-Guard Research Center funded by the Ministry of Science, ICT & Future Planning of Korea as "Global Frontier Project" (Grant number H-GUARD_2013M3A6B2078946).

Received: January 7, 2016
Revised: February 11, 2016
Published online: March 31, 2016

[1] a) N. Fujiwara, K. Kobayashi, *Curr. Drug Targets* **2005**, *4*, 281; b) H. Kosuge, S. P. Sherlock, T. Kitagawa, R. Dash, J. T. Robinson, H. Dai, M. V. McConnell, *J. Am. Heart Assoc.* **2012**, *1*, e002568; c) T. A. Wynn, A. Chawla, J. W. Pollard, *Nature* **2013**, *496*, 445.

[2] a) R. Choi, J. Yang, J. Choi, E. K. Lim, E. Kim, J. S. Suh, Y. M. Huh, S. Haam, *Langmuir* **2010**, *26*, 17520; b) Y. C. Liu, X. B. Zou, Y. F. Chai, Y. M. Yao, *Int. J. Biol. Sci.* **2014**, *10*, 520.

[3] a) S. K. Patel, J. M. Janjic, *Theranostics* **2015**, *5*, 150; b) P. W. Whitworth, C. C. Pak, J. Esgro, E. S. Kleinerman, I. J. Fidler, *Cancer Metastasis Rev.* **1990**, *8*, 319.

[4] E. J. Sanchez-Barcelo, M. D. Mediavilla, *Recent Pat. Endocr., Metab. Immune Drug Discovery* **2014**, *8*, 1.

[5] D. Jaque, L. M. Maestro, B. del Rosal, P. Haro-Gonzalez, A. Benayas, J. L. Plaza, E. M. Rodriguez, J. G. Sole, *Nanoscale* **2014**, *6*, 9494.

[6] a) X. J. Song, Q. Chen, Z. Liu, *Nano Res.* **2015**, *8*, 340; b) J. Fang, Y. C. Chen, *Curr. Pharm. Des.* **2013**, *19*, 6622.

[7] a) A. M. Alkilany, L. B. Thompson, S. P. Boulos, P. N. Sisco, C. J. Murphy, *Adv. Drug Delivery Rev.* **2012**, *64*, 190; b) S. Hwang, J. Nam, S. Jung, J. Song, H. Doh, S. Kim, *Nanomedicine* **2014**, *9*, 2003.

[8] E.-K. Lim, E. Jang, J. Kim, T. Lee, E. Kim, H. S. Park, J.-S. Suh, Y.-M. Huh, S. Haam, *J. Mater. Chem.* **2012**, *22*, 17518.

[9] a) P. L. McEuen, M. Fuhrer, H. Park, *IEEE Trans. Nanotechnol.* **2002**, *1*, 78; b) M. S. Dresselhaus, G. Dresselhause, R. Saito, *Carbon* **1995**, *33*, 883; c) P. R. Bandaru, *J. Nanosci. Nanotechnol.* **2007**, *7*, 1239; d) V. Popov, *Mater. Sci. Eng., R: Rep* **2004**, *43*, 61.

[10] W. Shao, P. Arghya, M. Yiyong, L. Rodes, S. Prakash. Carbon Nanotubes for Use in Medicine: Potentials and Limitations, *Syntheses and Applications of Carbon Nanotubes and Their Composites*, S. Suzuki. INTech, Reijeka, Croatia, **2013**, 285.

[11] a) Z. Liu, W. Cai, L. He, N. Nakayama, K. Chen, X. Sun, X. Chen, H. Dai, *Nat. Nanotechnol.* **2007**, *2*, 47; b) R. Toy, P. M. Peiris, K. B. Ghaghada, E. Karathanasis, *Nanomedicine* **2014**, *9*, 121; c) S. E. Gratton, P. A. Ropp, P. D. Pohlhaus, J. C. Luft, V. J. Madden, M. E. Napier, J. M. DeSimone, *Proc. Natl. Acad. Sci. USA* **2008**, *105*, 11613; d) P. M. Peiris, L. Bauer, R. Toy, E. Tran, J. Pansky, E. Doolittle, E. Schmidt, E. Hayden, A. Mayer, R. A. Keri, M. A. Griswold, E. Karathanasis, *ACS Nano* **2012**, *6*, 4157; e) K. R. Jain, *Cancer Metastasis Rev.* **1990**, *9*, 253.

[12] J. T. Robinson, K. Welsher, S. M. Tabakman, S. P. Sherlock, H. Wang, R. Luong, H. Dai, *Nano Res.* **2010**, *3*, 779.

[13] A. Dumas, P. Couvreur, *Chem. Sci.* **2015**, *6*, 2153.

[14] V. Shanmugam, S. Selvakumar, C. S. Yeh, *Chem. Soc. Rev.* **2014**, *43*, 6254.

[15] L. Belyanskaya, S. Weigel, C. Hirsch, U. Tobler, H. F. Krug, P. Wick, *Neurotoxicology* **2009**, *30*, 702.

[16] a) H. Kataura, Y. Maniwa, S. Masubuchi, S. Kazama, X. Zhao, Y. Ando, Y. Ohtsuka, S. Suzuki, Y. Achiba, R. Saito, *AIP Conf. Proc.* **2000**, *544*, 262; b) E. J. Park, N. E. Zahari, M. S. Kang, S. Lee, K. Lee, B. S. Lee, C. Yoon, M. H. Cho, Y. Kim, J. H. Kim, *Toxicol. Lett.* **2014**, *229*, 167.

[17] H. Maeda, H. Nakamura, J. Fang, *Adv. Drug Deliv. Rev.* **2013**, *65*, 71.

[18] a) N. Bertrand, J. Wu, X. Xu, N. Kamaly, O. C. Farokhzad, *Adv. Drug Deliv. Rev.* **2014**, *66*, 2; b) H. Maeda, *Adv. Drug Deliv. Rev.* **2015**, *91*, 3.

[19] a) W. X. Zhang, Z. Z. Zhang, Y. G. Zhang, *Nanoscale Res. Lett.* **2011**, *6*, 555; b) S. Vardharajula, *Int. J. Nanomed.* **2012**, *7*, 5361; c) V. Rastogi, P. Yadav, S. S. Bhattacharya, A. K. Mishra, N. Verma, A. Verma, J. K. Pandit, *J. Drug Delivery* **2014**, *2014*, 670815.

[20] T. Kwon, G. Lee, H. Choi, M. S. Strano, W. J. Kim, *Nanoscale* **2013**, *5*, 6773.

[21] M. H. Kim, B. Kim, E. K. Lim, Y. Choi, J. Choi, E. Kim, E. Jang, H. S. Park, J. S. Suh, Y. M. Huh, S. Haam, *Macromol. Biosci.* **2014**, *14*, 943.

[22] M. F. Linton, S. Fazio, *Curr. Opin. Lipidol.* **2001**, *12*, 489.

[23] P. J. Rice, J. L. Kelly, G. Kogan, H. E. Ensley, J. H. Kalbfleisch, I. W. Browder, D. L. Williams, *J. Leukocyte Biol.* **2002**, *72*, 140.

[24] a) M. S. S. Sergei, M. Bachilo, C. Kittrell, P. H. Hauge, R. E. Smalley, R. Bruce Weisman, *Science* **2012**, *298*, 2361; b) K. Jang, K. Eom, G. Lee, J.-H. Han, S. Haam, J. Yang, E. Kim, W.-J. Kim, T. Kwon, *BioChip J.* **2012**, *6*, 396.

[25] E. S. Jeng, C.-J. Shih, P. W. Barone, N. Jones, J. H. Baik, J. T. Abrahamson, M. S. Strano, *J. Phys. Chem. C* **2011**, *115*, 7164.

[26] Y. Tsubamoto, N. Yamada, Y. Watanabe, T. Inada, M. Shiomi, H. Shimano, T. Gotoda, K. Harada, M. Shimada, J. Ohsuga, M. Kawamura, Y. Yazaki, *Atherosclerosis* **1994**, *106*, 43.

[27] a) N. K. Mehra, V. Mishra, N. K. Jain, *Ther. Delivery* **2013**, *4*, 369; b) V. Ayala, A. P. Herrera, M. Latorre-Esteves, M. Torres-Lugo, C. Rinaldi, *J. Nanopart. Res.* **2013**, *15*, 1874.

[28] a) Y. C. Liu, X. B. Zou, Y. F. Chai, Y. M. Yao, *Int. J. Biol. Sci.* **2014**, *10*, 520; b) S. K. Patel, J. M. Janjic, *Theranostics* **2015**, *5*, 150.

[29] J. Kzhyshkowska, C. Neyen, S. Gordon, *Immunobiology* **2012**, *217*, 492.

[30] a) F. Charo, R. Taub, *Nat. Rev. Drug Discovery* **2011**, *10*. 365; b) G. K. Hansson, A. Hermansson, *Nat. Immunol.* **2011**, *12*. 204.

[31] G. P. István Kárpáti, É. Kovács, Z. Balogh, M. Szabolcs, J. Szabó, G. Kakuk, G. Fóris, *Nephrol. Dial. Transplant.* **1999**, *14*, 2664.

[32] C. Fournier, M. Leonard, E. Dellacherie, M. Chikhi, H. Hommel, A. P. Legrand, *J. Colloid Interface Sci.* **1998**, *198*, 27.